Langmuir

ARTICLE

pubs.acs.org/Langmuir

Tunable Wetting Mechanism of Polypyrrole Surfaces and Low-Voltage Droplet Manipulation via Redox

Yao-Tsan Tsai, Chang-Hwan Choi, Ning Gao, and Eui-Hyeok Yang*

Department of Mechanical Engineering, Stevens Institute of Technology, Hoboken, New Jersey 07030, United States

ABSTRACT: This paper presents the experimental results and analyses on a controlled manipulation of liquid droplets upon local reduction and oxidation (redox) of a smart polymer—dodecylbenzenesulfonate doped polypyrrole (PPy(DBS)). The electrochemically tunable wetting property of PPy(DBS) permitted liquid droplet manipulation at very low voltages (−0.9 to 0.6 V). A dichloromethane (DCM) droplet was flattened upon PPy(DBS) reduction. It was found that the surface tension gradient across the droplet contact line induced Marangoni stress, which caused this deformation. Further observation of PPy(DBS)'s color change upon the redox process confirmed that the surface tension gradient was the driving force for the droplet shape change.

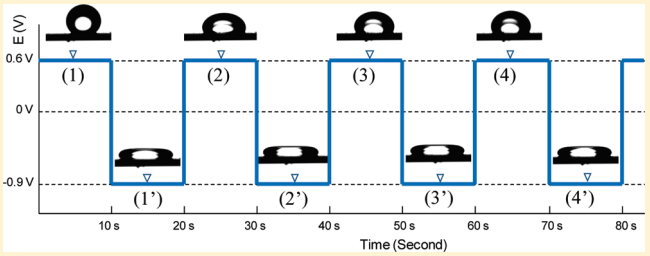

INTRODUCTION

Digital microfluidic systems have been developed in the past decade to generate and manipulate discrete droplets for biomedical applications.[1] By manipulating liquid at the droplet scale, these systems can handle samples and reagents with lower cost and shorter time for analysis using smaller devices.[2−4] At the microscale, droplet behavior is dominated by surface forces (e.g., surface tension or Laplace pressure) rather than body forces (e.g., gravity) due to high surface area-to-volume ratios.[5,6] For example, droplet manipulation has been used to generate net electromechanical force using the electrowetting effect on individually controlled electrodes.[7] However, such an electrostatic actuation scheme typically requires relatively high voltage (15−80 V) to manipulate liquid droplets.[8−14] Such high-voltage requirements have been major obstacles for clinical applications that demand portability and rapid diagnosis, where lower voltages are desirable for efficiency (e.g., using 1.5 V AA standard batteries). In addition, the high electric fields used for electrowetting effect could cause electrolysis on the working fluid in lab-on-a-chip applications.[15,16] While considerable efforts have been devoted to lowering the driving voltages required for electrowetting effect by using high-κ dielectric materials and ITO, it is still in the range of tens of volts.[17−19] As a direct alternative to the electrowetting mechanism, the surface energy of a polymer can be manipulated upon reduction and oxidization (redox) reactions at relatively low voltages (lower than 1 V).[20−24] A typical conjugated polymer experiences a change in its mechanical and electrical properties when "switched" (i.e., when undergoing a redox reaction), where the contact angle of a sessile droplet on the polymer surface depends on the applied oxidative potentials.[25−27] For example, dodecylbenzenesulfonate doped polypyrrole (PPy(DBS)) possesses maximum change of water contact angle between its reduced and oxidized states (e.g., 70−115°).[28,29] However, such investigation of tunable wetting properties of PPy(DBS) materials has been mostly performed at a single state configured discontinuously (i.e., only after either reduction or oxidation state). Further, there has been no systematic study of the droplet behavior during in situ continuous manipulation of PPy(DBS) for digital microfluidics. In this paper, we present experimental results on the in situ actuation of liquid droplets during a continuous redox process of a PPy(DBS) surface and an analysis of the droplet actuation mechanism. On the basis of the experimental measurement and analysis, we propose that a surface tension gradient across the contact line of a droplet, i.e., a resultant Marangoni stress, is the dominant driving mechanism in the low-voltage electrochemical droplet actuation upon the continuous redox of the PPy(DBS) surface. The PPy(DBS)-based electrochemical actuation enables ultra-low-voltage operation of droplets, and its unique surface properties are discussed for digital microfluidics applications.

EXPERIMENTAL METHODS

Fabrication of PPy(DBS). A PPy(DBS) film was fabricated using electropolymerization from aqueous monomer pyrrole solution.[27,30] An Au/Cr coated Si wafer was submerged in a freshly prepared pyrrole aqueous solution consisting of 0.1 M pyrrole (Aldrich) and 0.1 M sodium dodecylbenzenesulfonate (NaDBS) (Aldrich). The substrate was set as working electrode, and a saturated calomel electrode (SCE) (Fisher Scientific Inc.) and a platinum mesh were configured as reference and counter electrodes, respectively. A 263A potentiostat (Princeton Applied Research, Oak Ridge, TN) was used to potentiostatically deposit PPy(DBS) at +0.52 V vs SCE. The thickness of PPy(DBS) film was precisely controlled by adjusting the amount of applied charge. For instance, a 1 C cm^{-2} surface charge produces a 3 μm

Received: November 4, 2010
Revised: February 3, 2011

   dx.doi.org/10.1021/la104403w | *Langmuir* XXXX, XXX, 000–000

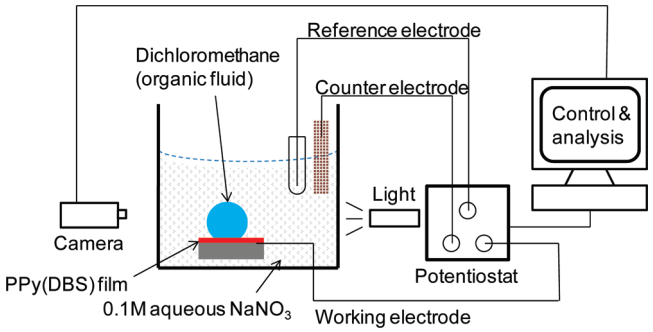

Figure 1. Schematic configuration of setup: electrochemical cell for PPy(DBS) redox within 0.1 M $NaNO_3$ aqueous solution.

thick PPy(DBS) film. After the PPy(DBS) film was deposited on the Au/Cr coated Si wafer, the substrate was rinsed with deionized (DI) water and dried.

Redox of PPy(DBS). The electrochemical behavior between the substrate and liquids was analyzed in a three-electrode system using cyclic voltammetry (CV) (263A, Princeton Applied Research). Cyclic voltammograms of PPy(DBS) were scanned from −1.0 V to +0.7 V in 0.1 M sodium nitrate ($NaNO_3$) aqueous solution for analyzing electrochemical reactions between PPy(DBS) and the electrolyte (50 mV s^{-1}). In addition, PPy(DBS) was scanned from −0.9 V to +0.6 V in pure dichloromethane (DCM) and 0.01 M $NaNO_3$-added DCM to examine any possible future electrochemical reaction between PPy(DBS) and DCM droplet. All potentials were recorded vs the SCE.

Contact Angle Measurement of Intrinsic Reduced and Oxidized PPy(DBS). The contact angles of DCM droplets on the reduced and oxidized PPy(DBS) film were measured in 0.1 M $NaNO_3$ aqueous solution, respectively. A goniometer/tensiometer (model 500, Rame-hart, Netcong, NJ) was used to measure the contact angle of a DCM droplet and the interfacial tension between DCM and electrolyte. A custom experimental setup was prepared to monitor droplet morphology on PPy(DBS) within the aqueous environment as shown in Figure 1. Here, the ~200 nm thick PPy(DBS) film-coated substrate was placed in a transparent flask in a 0.1 M $NaNO_3$ aqueous solution. An SCE and a platinum mesh were connected as reference and counter electrodes, respectively. An oxidative potential (+0.6 V vs SCE) was applied to the substrate through the working electrode. The DCM droplet was then dispensed on the oxidized PPy(DBS) surface and the contact angle of the droplet was measured. After removing the first droplet, a reductive potential (−0.9 V vs SCE) was applied on the substrate, and a new DCM droplet was dispensed on the reduced PPy(DBS) film and its contact angle was measured.

Droplet Motion upon Continuous Reduction and Oxidation Reactions. The same setup was used to monitor a single DCM droplet behavior continuously, while redox reactions were performed on the PPy(DBS) film (Figure 1). Initially an oxidative potential (+0.6 V vs SCE) was applied on the PPy(DBS) substrate to increase adhesion between the DCM droplet and PPy(DBS) film. Then, the DCM droplet was dispensed on the PPy(DBS) in a 0.1 M $NaNO_3$ aqueous environment using a dispensing syringe (ca. 1−5 μL). The working electrode potential was adjusted between −0.9 V and +0.6 V vs SCE using a potentiostat (263A, Princeton Applied Research) (Pulse length: 10 s). The shape of the droplet and the change of contact angle upon the repetitive PPy(DBS) redox was monitored and recorded for 100 cycles.

RESULTS AND DISCUSSION

Cyclic Voltammetry of PPy(DBS). The cyclic voltammogram (CV) in Figure 2a shows potentiodynamic reduction and oxidation reactions of PPy(DBS) in a 0.1 M $NaNO_3$ aqueous solution.

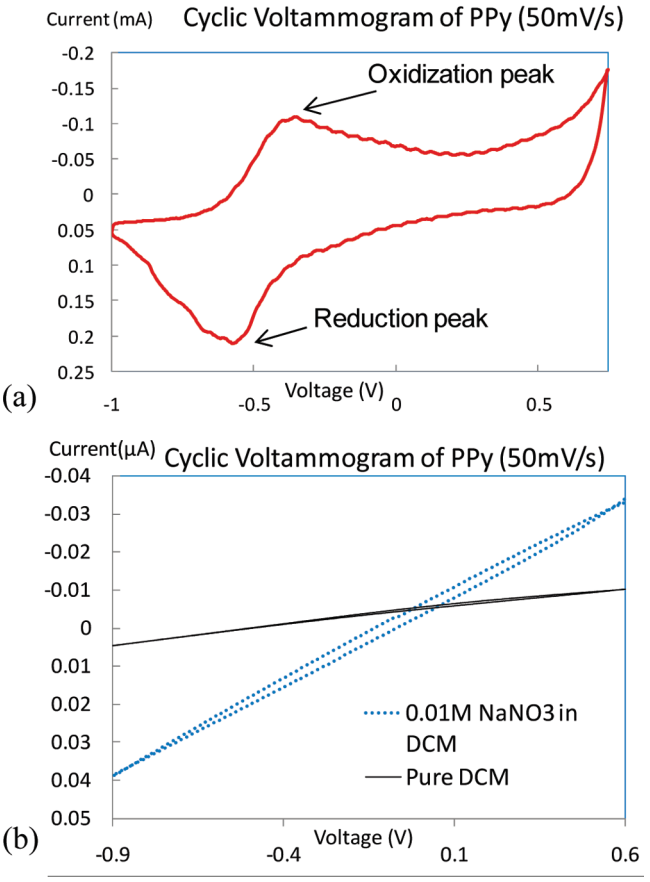

Figure 2. (a) A cyclic voltammogram shows the reduction-oxidization reaction of PPy(DBS) in 0.1 M $NaNO_3$ aqueous solution. (b) Cyclic voltammograms of PPy(DBS) in pure DCM and DCM mixed with 0.01 M $NaNO_3$, respectively.

The CV indicates that there was an oxidization peak at −0.4 V and a reduction peak at −0.6 V. For the oxidization reaction, the current was stable when the potential was between 0.2 and 0.6 V, suggesting that the oxidization reaction was completed; however, the current suddenly increased when the potential was greater than 0.6 V, indicating that a side reaction started to occur. The reduction reaction was completed when the potential was less than −0.7 V. For a complete redox reaction in our experiments, 0.6 V and −0.9 V were chosen as the upper and lower limits of electric potential, respectively.

The CV test of PPy(DBS) within pure DCM was performed to confirm if any electrochemical reaction was existing between PPy(DBS) and DCM when potentials were applied to the film. The 0.01 M $NaNO_3$-added DCM was also tested to examine any possible diffusion of $NaNO_3$ into DCM as an ion provider for PPy(DBS) redox. The comparison of CV of the PPy(DBS) film between pure DCM and DCM mixed with 0.01 M $NaNO_3$ is shown in Figure 2b. The results indicate no specific peak in the CV curves, indicating that there was no electrochemical reaction of PPy(DBS) with either condition of DCM in the range between +0.6 V and −0.9 V.

Intrinsic Wetting Property of Reduced and Oxidized PPy(DBS). The surface state of PPy(DBS) can be "tuned" from hydrophilic to hydrophobic via reorientation of its surfactant dopant molecules, dodecylbenzenesulfonate (DBS).[31] When an oxidative potential is applied to PPy(DBS), sodium (Na^+) ions

dx.doi.org/10.1021/la104403w |*Langmuir* XXXX, XXX, 000–000

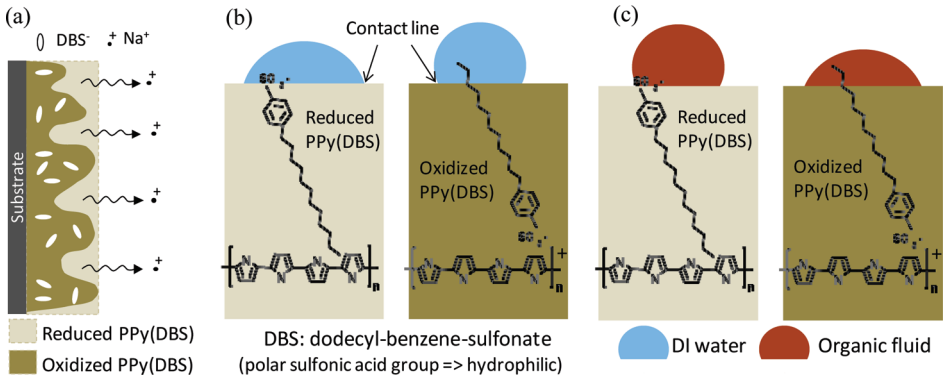

Figure 3. Surface state of PPy(DBS) bidirectionally "tuned" from hydrophilic to hydrophobic: (a) When the PPy(DBS) is oxidized, sodium (Na^+) ions are diffused out from the PPy(DBS) surface for charge neutralization, while DBS^- molecules are immobilized. (b) Oxidization of PPy(DBS) film lowers the surface energy and increases the contact angle of a water droplet (hydrophobic). (c) In the case of an organic fluid such as DCM, the contact angle of a droplet is decreased on oxidized PPy(DBS) surface (oleophilic).

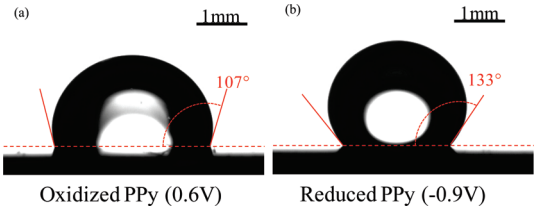

Figure 4. DCM droplets on PPy(DBS) films within 0.1 M $NaNO_3$ aqueous solution: (a) oxidized state (+0.6 V vs SCE) (contact angle ~107°); (b) reduced state (−0.9 V vs SCE) (contact angle ~133°). After removing the first droplet, a new DCM droplet was dispensed on the reduced PPy(DBS) film. When the surface state changes from an oxidized to reduced state, the droplet height increases and the contact radius (r_c) decreases due to the increased contact angle.

are repelled from the PPy(DBS) surface for charge neutralization, leaving behind immobilized DBS^- molecules (Figure 3a).[32,33] Likewise, Na^+ ions need to enter into PPy for charge neutralization upon reduction. In the oxidized PPy(DBS), DBS^- molecules are coupled to PPy chains via ionic bonding with polar sulfonic acid group, allowing the dodecyl chains to be thrust out from the polymer chains. Since the strongly hydrophilic polar sulfonic acid group is attracted to the polymer backbone and the hydrophobic amine group is heading out to the surface, the surface becomes hydrophobic and the contact angle of a water droplet on an oxidized PPy(DBS) film is increased (Figure 3b).[23] On the other hand, a nonpolar liquid such as DCM shows opposite wetting states, i.e., lower contact angle on the oxidized PPy(DBS) surface than on the reduced one due to its higher oleophilicity (Figure 3c).[34,35]

The contact angle of the DCM droplet measured on oxidized PPy(DBS) surface ($\theta_{oxi} \approx 107°$) is shown in Figure 4a. After removing the first droplet, a reductive potential (−0.9 V vs SCE) was applied on the substrate, and a new DCM droplet was dispensed on the reduced PPy(DBS) film. The DCM droplet exhibited a higher contact angle on the reduced PPy(DBS) surface ($\theta_{red} \approx 133°$) (Figure 4b). After the PPy(DBS) surface was converted from the oxidized state to reduced state, the surface became hydrophilic (or oleophobic) and resulted in an increase of a height and a decrease of a contact radius of the DCM droplet. The height of DCM drops was increased by 19% and the contact radius was decreased by 30% when the contact angle was changed from 107° to 133°.

Droplet Actuation upon Continuous Reduction and Oxidation Reactions. In contrast to the separate measurement of the intrinsic wetting states of DCM droplets for each redox state, "continuous" electrochemical tuning was performed by applying a square pulse potential to the PPy(DBS) substrate to investigate DCM droplet behavior. When a reductive potential (−0.9 V vs SCE) was applied to the oxidized PPy(DBS) film with a DCM drop on top, the spherical DCM droplet was flattened with little change of the contact angle and its height was reduced by 65%. (Figure 5). Due to this flattening effect, the baseline diameter of DCM droplet was increased upon application of a reductive potential. Upon the application of oxidative potentials (Figure 5: state (1′) to (2), (2′) to (3), and (3′) to (4)), the droplet returned to a spherical shape. This reversible switching phenomenon was maintained for 20−30 cycles. This droplet flattening behavior in continuous redox reaction was different from the intrinsic wetting property discussed in the previous section, suggesting that the droplet actuation in continuous redox process was not driven by the contact angle change.

This "droplet spreading" phenomenon was previously observed by Halldorsson et al.[24] using a DCM droplet placed on a PPy(DBS) coated mesh. The droplet spreading behavior was explained as the movement of DBS^- anions into a DCM droplet during the reduction of the PPy(DBS). According to this report, DBS^- acted as a surfactant to decrease the DCM−electrolyte surface tension, thereby inducing droplet spreading. However, such speculation is not conclusive since DBS^- molecules are relatively immobilized during PPy(DBS) redox.[23,24,27] The droplet spreading occurs quite rapidly (<1 s) as observed in our experiments, and the relatively immobilized DBS^- molecules cannot effectively diffuse into a DCM droplet for charge neutralization in such a short interval. It also suggests that the actuation of DCM droplet should be driven by the other effects.

Effects of Marangoni Stress. Since DBS^- molecules are relatively immobilized anions, the charge neutralization during PPy(DBS) redox is dominated by the transportation of cations (Na^+) in electrolyte.[24,36] For complete reduction of PPy(DBS) film, sodium ions (Na^+) in the electrolyte need to transport into PPy(DBS) for charge neutralization.[27] As illustrated in Figure 6a, no such ion would be available at the "contact zone" (i.e., the area covered by the DCM droplet) when the reductive potential is applied. This is because $NaNO_3$ has low solubility in DCM, as confirmed by the CV (Figure 2b) showing that there was no electrochemical reaction between PPy(DBS) and DCM. The

dx.doi.org/10.1021/la104403w |*Langmuir* XXXX, XXX, 000–000

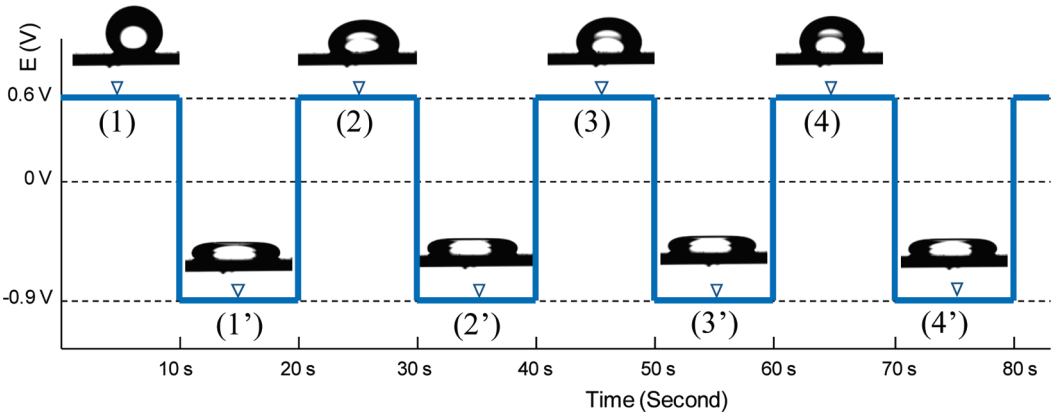

Figure 5. DCM droplet dispersed on a PPy(DBS) film in a three-electrode setup containing 0.1 M $NaNO_3$ aqueous solution: Square pulse potential (−0.6 to 0.9 V) was applied to the substrate for PPy(DBS) redox (Pulse length: 10 s). The DCM droplet was flattened to a "disk-like" shape while the PPy(DBS) was reduced from oxidized state (i.e., (1) to (1′), (2) to (2′), (3) to (3′), and (4) to (4′)). The DCM droplet returned to a spherical shape while the PPy(DBS) returned to oxidized state (i.e., (1′) to (2), (2′) to (3), and (3′) to (4)).

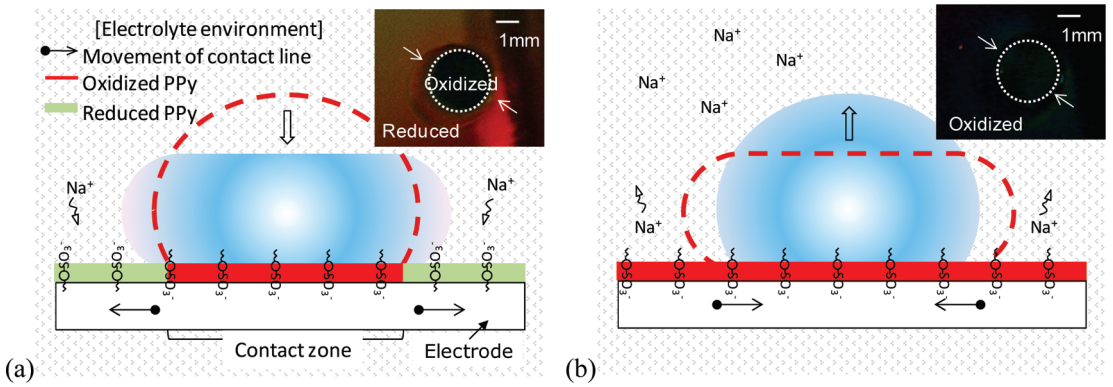

Figure 6. (a) Surface tension gradient and Marangoni stress are induced due to the lack of sodium ions for PPy(DBS) reduction underneath the DCM droplet. When a PPy(DBS) substrate is reduced, the polymer substrate underneath the DCM droplet is still in the oxidized state. The contact line moves outward due to Marangoni stress and the droplet is flattened to disk-like shape. (Inset) Top view of DCM droplet on the reduced PPy(DBS) substrate; PPy(DBS) film transforms into a brown color except the area blocked by the DCM droplet. The arrows indicate the periphery of the DCM droplet, and the white dotted circle indicates the contact line. (b) Marangoni stress vanishes when the PPy(DBS) film is oxidized. The DCM droplet reverts to spherical shape by internal Laplace pressure gradient to minimize its surface energy. (Inset) Top view of DCM droplet on an oxidized PPy(DBS) substrate; the whole PPy(DBS) film becomes dim, which indicates that the surface tension gradient has vanished.

blockage of the PPy(DBS) reduction at the contact zone creates heterogeneous surface states (or localized reduction) across the droplet contact line. Then, the surface tension gradient created across the contact line upon a localized reduction of the PPy-(DBS) induces Marangoni stress. The Marangoni stress causes the liquid to move away from a region of low surface tension toward a region of high surface tension.[37,38] The reduced PPy-(DBS) has higher surface energy and our results show that the baseline of DCM droplet increases when the PPy(DBS) film is reduced (Figure 5: State (1) to (1′), (2) to (2′), (3) to (3′), and (4) to (4′)).

Further evidence comes from the color change of PPy(DBS) upon reduction and oxidation: A thin PPy(DBS) film (<1 μm) on a gold substrate is a brown color in the reduced state, while it is dim/dark in the oxidized state.[39] The inset in Figure 6a shows the top view of a DCM droplet on the reduced PPy(DBS) substrate (note that PPy(DBS) underneath the DCM still remains oxidized). The dotted circle indicates a contact line at the reduction of the PPy(DBS). As shown in the inset of Figure 6a, PPy(DBS) film was brown (i.e., reduced state) except in the dark central circular area underneath the DCM droplet. The different color of PPy(DBS) film across the contact line indicates that the circular area of PPy(DBS) underneath the DCM droplet was in the oxidized state while the external PPy(DBS) was in the reduced state. Since reduced PPy(DBS) possesses higher surface energy, this observation of color change clearly illustrates the surface tension gradient across the contact line.

Figure 6b shows the case that the PPy(DBS) substrate is switched back to oxidized state (Figure 5: state (1′) to (2), (2′) to (3), and (3′) to (4)). When an oxidative potential was applied, the PPy(DBS) film retained a homogeneous oxidized state and the surface tension gradient was eliminated. Consequently, the induced Marangoni stress faded and the DCM droplet returned back to a spherical shape to minimize its surface energy. The inset in Figure 6b gave the top view of the DCM droplet on the oxidized PPy(DBS) substrate, where no significant gradient of color across the contact line was observable, indicating that the film was in the homogeneously oxidized state.

Analysis of Droplet Actuation Force Induced by Marangoni Stress. The proposed driving mechanism is further

dx.doi.org/10.1021/la104403w |*Langmuir* XXXX, XXX, 000–000

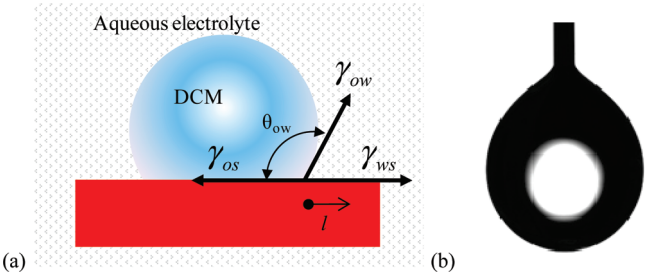

Figure 7. (a) Equilibrium of interfacial forces on a DCM droplet placed within aqueous electrolyte. (b) Pendant drop of DCM in 0.1 M $NaNO_3$ aqueous solution for interfacial tension measurement. The measured interfacial tension between DCM and 0.1 M $NaNO_3$ aqueous solution is $\gamma_{ow} = 26.54 \pm 0.51$ mN m^{-1}. (27 measurements were performed.)

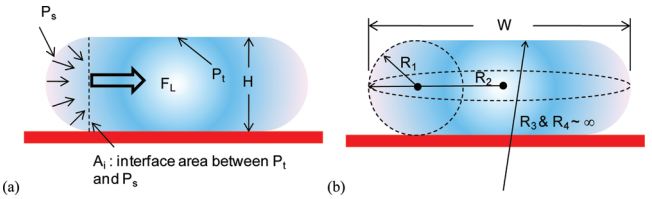

Figure 8. (a) Pressure gradient inside a nonspherical droplet due to the nonuniform radius of curvature of a droplet profile. The internal pressure is described by the Laplace law.[38] (b) R_1 and R_2 are the horizontal and vertical curvature radii at the edge of the droplet, respectively; R_3 and R_4 are the horizontal and vertical curvature radii at the top center of the droplet, respectively.

confirmed by force analysis on the dispensed droplet. The force induced by Marangoni stress is balanced with the force which creates a pressure difference within the droplet. The pressure difference can be calculated using the radius of curvature based on the Young−Laplace equation.[38] First, the induced Marangoni stress can be obtained as the following: Bartell−Osterhof equation (eq 1) presents the relationship between contact angle and interfacial tension for solid−liquid−liquid system (Figure 7a).

$$\gamma_{ow} \cos \theta_{ow} = \gamma_o \cos \theta_{os} - \gamma_w \cos \theta_{ws} \quad (1)$$

where γ_{ow} is the interfacial tension between DCM and 0.1 M $NaNO_3$ solution, γ_o and γ_w are the interfacial tension between DCM−air and electrolyte−air, respectively, θ_{ow} is the contact angle of a DCM droplet within 0.1 M $NaNO_3$ aqueous environment, θ_{os} and θ_{ws} are the contact angles of DCM and electrolyte droplets in the air, respectively. Upon application of reductive (or oxidative) potential, surface energy is changed while interfacial tension between electrolyte and DCM remains unchanged.[40] The variation of surface tension between the reduced PPy(DBS) and the oxidized PPy(DBS) can be obtained by[41,42]

$$\Delta\gamma = \gamma_{ow} \cos \theta'_{ow} - \gamma_{ow} \cos \theta_{ow} = \gamma_{ow}(\cos \theta'_{ow} - \cos \theta_{ow}) \quad (2)$$

where θ'_{ow} is the contact angle of DCM droplet within 0.1 M $NaNO_3$ aqueous environment on the switched PPy(DBS). The interfacial tension of the DCM-electrolyte was measured by the pendant drop method,[43] where interfacial tension between two immiscible liquids can be calculated from the profile of a static pendant drop (Figure 7b). A total of 27 measurements were performed for measuring interfacial tension of DCM-electrolyte (γ_{ow}). The average value was 26.54 mN m^{-1} and the standard deviation was 0.51 mN m^{-1}. Further, the Marangoni stress, τ, can be derived from surface tension gradient.[38]

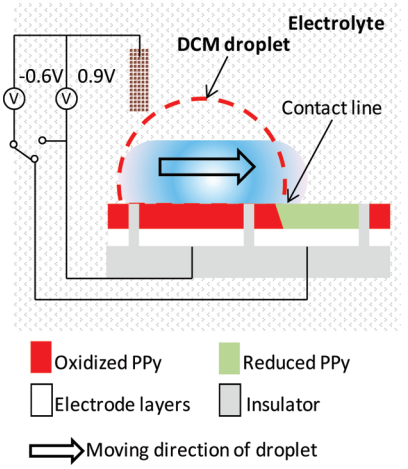

Figure 9. A DCM droplet is dispensed on preoxidized PPy(DBS) patterned electrodes. Negative voltage is applied to reduce the PPy-(DBS) film on the activated electrode. The PPy(DBS) substrate under the DCM droplet remains oxidized, and thus the droplet contact line touching the reduced areas will move toward them due to Marangoni stress.

$$\tau = \frac{\partial \gamma}{\partial l} \quad (3)$$

where l is the transition length of surface tension variation. Therefore, the unbalanced force induced from the Marangoni stress is

$$F_\gamma = \tau \times A = \frac{\partial \gamma}{\partial l} \times (dl \times s) = \Delta\gamma \times s$$
$$= \Delta\gamma \times 2\pi \times (W - H) \quad (4)$$

where s is the periphery of the contact line between liquid droplet and PPy(DBS), and W and H are the measured width and height of the droplet using goniometer, respectively (Figure 8), dl is the displacement of contact line upon PPy-(DBS) redox.[42,44] For the case of a 4.93 μL droplet ((1′) in Figure 5), the measured W and H were 3.9 mm and 0.614 mm, respectively. Using the measured interfacial tension of the DCM-electrolyte, γ_{ow}, the calculated force induced by Marangoni stress is approximately 10^{-4} N when the contact angle is changed from 107° to 133°.

Meanwhile, when a droplet is flattened, a pressure gradient (ΔP, eq 5) is created inside the droplet due to the nonuniform radius of curvature of the droplet (Figure 8),[38] such as

$$\Delta P = P_s - P_t = \gamma_{ow}\left(\frac{1}{R_1} + \frac{1}{R_2}\right) - \gamma_{ow}\left(\frac{1}{R_3} + \frac{1}{R_4}\right) \quad (5)$$

$$F_L = \Delta P \times A_i = \Delta P \times H \times \pi \times (W - H) \quad (6)$$

The pressure gradient induces an unbalanced force, F_L, which is estimated as the following: Laplace pressure, P_s, in the region of the droplet edge is larger than the Laplace pressure, P_t, at the center of a droplet because the droplet possesses a smaller radius of curvature at the edge. For the case of (1′) in Figure 5,

dx.doi.org/10.1021/la104403w |*Langmuir* XXXX, XXX, 000–000

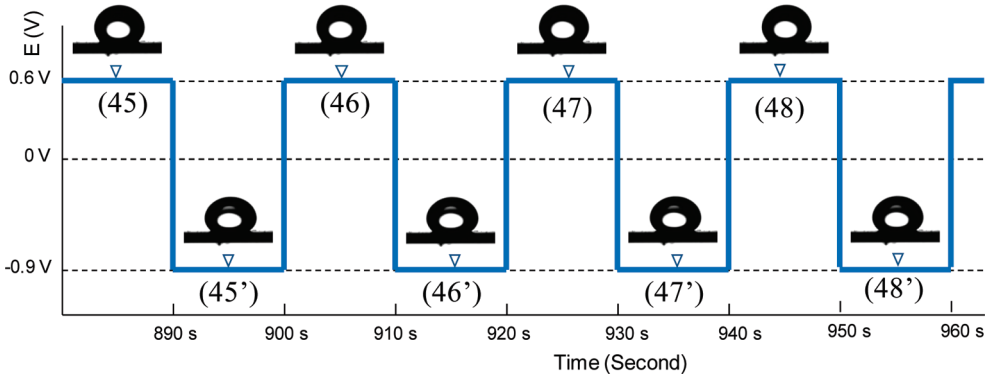

Figure 10. DCM droplet manipulation upon continuous redox (cycle 45 to 48). The DCM droplet exhibited minor deformation.

$R_1 = H/2 = 0.307$ mm, $R_2 = W/2 = 1.95$ mm, R_3 and R_4 were infinite, respectively. A_i was the interface area between P_s and P_t, i.e., the surface area of the cylinder with the radius of $W - H$. Using eqs 5 and 6, the estimated force F_L induced by the pressure gradient is on the order of 10^{-4} N, which is comparable to the induced force by the Marangoni stress. This analysis also supports the hypothesis that the major driving mechanism for the droplet deformation during the continuous PPy(DBS) redox reaction is Marangoni stress.

It is envisioned that liquid droplets within an electrolyte solution can be individually manipulated by the electrically triggered Marangoni effect on a PPy(DBS) film fabricated on patterned conducting electrodes in the manner similar to the architectures typically used in digital microfluidic systems as shown in Figure 9.

Pinning Effects. After approximately 30 cycles of continuous actuation of the DCM droplet, the droplet did not exhibit the disk-like deformation any longer. Instead, the contact line of DCM droplet was pinned on the PPy(DBS) surface and the contact radius did not change upon PPy(DBS) redox (Figure 10). This is believed to be due to the pinning of DCM on the PPy(DBS) film during the repeated redox reactions over a period of time (>3 min). When the PPy(DBS) is oxidized, adhesion between oxidized PPy(DBS) and DCM is increased because the oxidized PPy(DBS) is more oleophilic. Therefore, DCM molecules start aggregating on the PPy(DBS) surface and form a thin film. Eventually the droplet's baseline is pinned on the surface and the droplet actuation is significantly retarded by the pinning effects.

Pinning is a common and challenging issue for microfluidic devices.[16,45−49] One can avoid pinning by reducing contact duration between DCM and PPy(DBS). In most droplet-based digital microfluidics, a droplet is continuously transported with short residence time on the same spot (e.g., much less that 3 min).[46] Therefore, such a pinning problem would not be a critical issue for the continuous operation of a digital microfluidic device if the droplet resident lifetime on the PPy(DBS) surface is shorter than the critical contact time for significant molecular adsorption. However, if the droplet is manipulated repeatedly on the same spot on the device, it will eventually be pinned at the contact line due to the pinning effects. In this case, the increased surface friction due to the contact line pinning will hamper efficient droplet manipulation driven by the Marangoni stress. To overcome such a problem, one can introduce micro/nano patterns such as line, pillar, or pore patterns in PPy(DBS) surface to reduce the overall contact area, which can considerably reduce pinning during the droplet manipulation.[50−55]

CONCLUSIONS

In this study, manipulation of a liquid droplet at low voltage (−0.9 to 0.6 V) has been demonstrated using tunable wetting properties of conjugated polymers. Further, the droplet behaviors upon discontinuous vs continuous PPy(DBS) redox processes have been discussed. Marangoni stress was found to be the major driving mechanism for manipulation of a droplet's meniscus upon continuous PPy(DBS) reduction and oxidation reactions. The electrochemical redox process on smart polymers reported in this paper can be applied to a low voltage manipulation of liquid droplets for microfluidic applications to realize their full potential in rapid diagnosis applications.

AUTHOR INFORMATION

Corresponding Author

*Corresponding author. E-mail: Eui-Hyeok.Yang@stevens.edu. Phone: 201-216-5574. Fax: 201-216-8315.

ACKNOWLEDGMENT

This research has been partially carried out in part at the Center for Functional Nanomaterials, Brookhaven National Laboratory, which is supported by the U.S. Department of Energy, Office of Basic Energy Sciences, under contract no. DE-AC02-98CH10886. The authors also thank Kitu Kumar for her assistance in revising the paper.

REFERENCES

(1) Squires, T. M.; Quake, S. R. Microfluidics: Fluid physics at the nanoliter scale. *Rev. Mod. Phys.* **2005**, *77* (3), 977–1026.

(2) Daw, R.; Finkelstein, J. Lab on a chip. *Nature* **2006**, *442* (7101), 367–367.

(3) Stone, H. A.; Stroock, A. D.; Ajdari, A. Engineering flows in small devices: Microfluidics toward a lab-on-a-chip.*Annu. Rev. Fluid Mech.* **2004**, *36*, 381−411.

(4) Whitesides, G. M. The origins and the future of microfluidics. *Nature* **2006**, *442* (7101), 368–373.

(5) Darhuber, A. A.; Troian, S. M. Principles of microfluidic actuation by modulation of surface stresses. *Annu. Rev. Fluid Mech.* **2005**, *37*, 425−455.

(6) Sumino, Y.; Magome, N.; Hamada, T.; Yoshikawa, K. Self-running droplet: emergence of regular motion from nonequilibrium noise. *Phys. Rev. Lett.* **2005**, *94* (6), 068301.
(7) Jones, T. B. On the relationship of dielectrophoresis and electrowetting. *Langmuir* **2002**, *18* (11), 4437–4443.
(8) Teh, S. Y.; Lin, R.; Hung, L. H.; Lee, A. P. Droplet microfluidics. *Lab Chip* **2008**, *8* (2), 198.
(9) Quilliet, C.; Berge, B. Electrowetting: A recent outbreak. *Curr. Opin. Colloid Interface Sci.* **2001**, *6* (1), 34–39.
(10) Mugele, F.; Baret, J. C. Electrowetting: From basics to applications. *J. Phys.: Condens. Matter* **2005**, *17* (28), R705–R774.
(11) Lienemann, J.; Greiner, A.; Korvink, J. G. Modeling, simulation, and optimization of electrowetting. *IEEE Trans. Comput.-Aided Des. Integrated Circuits Syst.* **2006**, *25* (2), 234–247.
(12) Gaurav, J. S.; Aaron, T. O.; Eric, P. Y. C.; Ming, C. W.; Chang-Jin, J. K. EWOD-driven droplet microfluidic device integrated with optoelectronic tweezers as an automated platform for cellular isolation and analysis. *Lab Chip* **2009**, *9* (12), 1732–1739.
(13) Berthier, J.; Dubois, P.; Clementz, P.; Claustre, P.; Peponnet, C.; Fouillet, Y. Actuation potentials and capillary forces in electrowetting based microsystems. *Sens. Actuators, A* **2007**, *134* (2), 471–479.
(14) He, R.; Kim, C. J. A low temperature vacuum package utilizing porous alumina thin film encapsulation; *Proceedings of the IEEE International Conference on Micro Electro Mechanical Systems (MEMS)*, Istanbul, 2006; pp 126−129.
(15) Stefan, H.; Roland, Z. Microfluidic platforms for lab-on-a-chip applications. *Lab Chip* **2007**, *7* (9), 1094–1110.
(16) Fair, R. B. Digital microfluidics: is a true lab-on-a-chip possible?. *Microfluid. Nanofluid.* **2007**, *3* (3), 245.
(17) Moon, H.; Cho, S. K.; Garrell, R. L.; Kim, C. J. Low voltage electrowetting-on-dielectric. *J. Appl. Phys.* **2002**, *92* (7), 4080.
(18) Yun, K. S.; Kim, C. J. Low-voltage elctrostatic actuation of droplet on thin superhydrophobic nanoturf. In *Proceedings of the IEEE International Conference on Micro Electro Mechanical Systems (MEMS)*, Kobe, 2007; pp 139−142.
(19) Vasudev, A.; Zhe, J. A low voltage capillary microgripper using electrowetting; TRANSDUCERS 2009 - 15th International Conference on Solid-State Sensors, Actuators and Microsystems, Denver, CO, 2009; pp 825−828.
(20) Gallardo, B. S.; Gupta, V. K.; Eagerton, F. D.; Jong, L. I.; Craig, V. S.; Shah, R. R.; Abbott, N. L. Electrochemical principles for active control of liquids on submillimeter scales. *Science* **1999**, *283* (5398), 57–60.
(21) Causley, J.; Stitzel, S.; Brady, S.; Diamond, D.; Wallace, G. Electrochemically-induced fluid movement using polypyrrole. *Synth. Met.* **2005**, *151* (1), 60–64.
(22) Isaksson, J.; Robinson, N. D.; Berggren, M. Electronic modulation of an electrochemically induced wettability gradient to control water movement on a polyaniline surface. *Thin Solid Films* **2006**, *515* (4), 2003–2008.
(23) Isaksson, J.; Tengstedt, C.; Fahlman, M.; Robinson, N.; Berggren, M. A solid state organic electronic wettability switch. *Adv. Mater.* **2004**, *16* (4), 316–320.
(24) Halldorsson, J. A.; Little, S. J.; Diamond, D.; Spinks, G.; Wallace, G. Controlled transport of droplets using conducting polymers. *Langmuir* **2009**, *25* (18), 11137–11141.
(25) Wallace, G. G.; Spinks, G. M.; Kane-Maguire, L. A. P.; Teasdale, P. R. *Conductive Electroactive Polymers: Intelligent Polymer Systems*, 3rd ed.; CRC Press: Boca Raton, 2008.
(26) Tietje-Girault, J.; Ponce de Leon, C.; Walsh, F. C. Electrochemically deposited polypyrrole films and their characterization. *Surf. Coat. Technol.* **2007**, *201* (12), 6025–6034.
(27) Smela, E. Microfabrication of PPy microactuators and other conjugated polymer devices. *J. Micromech. Microeng.* **1999**, *9* (1), 1–18.
(28) Teh, K. S.; Takahashi, Y.; Yao, Z.; Lu, Y.-W. Influence of redox-induced restructuring of polypyrrole on its surface morphology and wettability. *Sens. Actuators, A* **2009**, *155* (1), 113–119.
(29) Takahashi, Y.; Teh, K. S.; Lu, Y. W. Wellability switching technique of a biocompatible polymer; *Proceedings of the IEEE International Conference on Micro Electro Mechanical Systems (MEMS)*, 2009; pp 459−462.
(30) Tsai, Y. T.; Choi, C. H.; Yang, E. H. Droplet actuation in PPy redox process; TechConnect World Conference and Expo, Anaheim, CA; Jun 21−25, 2010; pp 476−479.
(31) Xu, L.; Chen, W.; Mulchandani, A.; Yan, Y. Reversible conversion of conducting polymer films from superhydrophobic to superhydrophilic13. *Angew. Chem., Int. Ed.* **2005**, *44* (37), 6009–6012.
(32) Torresi, R. M.; Córdoba de Torresi, S. I.; Matencio, T.; De Paoli, M. A. Ionic exchanges in dodecylbenzenesulfonate-doped polypyrrole Part II: Electrochemical quartz crystal microbalance study. *Synth. Met.* **1995**, *72* (3), 283–287.
(33) Matencio, T.; De Paoli, M. A.; Peres, R. C. D.; Torresi, R. M.; Cordoba de Torresi, S. I. Ionic exchanges in dodecylbenzenesulfonate doped polypyrrole Part 1. Optical beam deflection studies. *Synth. Met.* **1995**, *72* (1), 59–64.
(34) Lim, T. T.; Huang, X. In situ oil/water separation using hydrophobic-oleophilic fibrous wall: A lab-scale feasibility study for groundwater cleanup. *J. Hazardous Mater.* **2006**, *137* (2), 820–826.
(35) Zhang, J.; Huang, W.; Han, Y. A composite polymer film with both superhydrophobicity and superoleophilicity. *Macromol. Rapid Commun.* **2006**, *27* (10), 804–808.
(36) Skaarup, S.; Bay, L.; Vidanapathirana, K.; Thybo, S.; Tofte, P.; West, K. Simultaneous anion and cation mobility in polypyrrole. *Solid State Ionics* **2003**, *159* (1−2), 143–147.
(37) Nikolov, A. D.; Wasan, D. T.; Chengara, A.; Koczo, K.; Policello, G. A.; Kolossvary, I. Superspreading driven by Marangoni flow. *Adv. Colloid Interface Sci.* **2002**, *96* (1−3), 325–338.
(38) Berthier, J. *Microdrops and Digital Microfluidics*; William Andrew Inc.: Norwick, NY, 2008; p 350.
(39) Wang, X.; Smela, E. Color and volume change in PPy(DBS). *J. Phys. Chem. C* **2008**, *113* (1), 359–368.
(40) Maillard, M.; Legrand, J.; Berge, B. Two liquids wetting and low hysteresis electrowetting on dielectric applications. *Langmuir* **2009**, *25* (11), 6162–6167.
(41) Brochard, F. Motions of droplets on solid surfaces induced by chemical or thermal gradients. *Langmuir* **1989**, *5* (2), 432–438.
(42) Lee, S.-W.; Laibinis, P. E. Directed movement of liquids on patterned surfaces using noncovalent molecular adsorption. *J. Am. Chem. Soc.* **2000**, *122* (22), 5395–5396.
(43) Andreas, J. M.; Hauser, E. A.; Tucker, W. B. Boundary tension by pendant drops. *J. Phys. Chem.* **1938**, *42* (7), 1001–1019.
(44) Chaudhury, M. K.; Whitesides, G. M. How to make water run uphill. *Science* **1992**, *256* (5063), 1539–1544.
(45) Mukhopadhyay, R. When microfluidic devices go bad. *Anal. Chem.* **2005**, *77* (21), 429A–432A.
(46) Yoon, J. Y.; Garrell, R. L. Preventing biomolecular adsorption in electrowetting-based biofluidic chips. *Anal. Chem.* **2003**, *75* (19), 5097–5102.
(47) Han, J.-H.; Yoon, J.-Y. Reusable, polyethylene glycol-structured microfluidic channel for particle immunoassays. *J. Biol. Eng.* **2009**, *3* (1), 6.
(48) Nanayakkara, Y. S.; Moon, H.; Payagala, T.; Wijeratne, A. B.; Crank, J. A.; Sharma, P. S.; Armstrong, D. W. A fundamental study on electrowetting by traditional and multifunctional ionic liquids: possible use in electrowetting on dielectric-based microfluidic applications. *Anal. Chem.* **2008**, *80* (20), 7690–7698.
(49) Fair, R. B.; Srinivasan, V.; Ren, H.; Paik, P.; Pamula, V. K.; Pollack, M. G. In *Electrowetting-Based On-Chip Sample Processing for Integrated Microfluidics*, Washington, DC, 2003; pp 779−782.
(50) Rothstein, J. P. Slip on superhydrophobic surfaces. *Annu. Rev. Fluid Mech.* **2010**, *42* (1), 89–109.
(51) Quere, D. Wetting and roughness. *Annu. Rev. Mater. Res.* **2008**, *38* (1), 71–99.
(52) Petrie, R. J.; Bailey, T.; German, C. B.; Genzer, J. Fast directed motion of "Fakir" droplets. *Langmuir* **2004**, *20* (23), 9893–9896.

(53) Quere, D. Surface chemistry: Fakir droplets. *Nat. Mater.* **2002**, *1* (1), 14–15.
(54) de Gennes, P. G. Wetting: statics and dynamics. *Rev. Mod. Phys.* **1985**, *57* (3), 827.
(55) Rauscher, M.; Dietrich, S. Wetting phenomena in nanofluidics. *Annu. Rev. Mater. Res.* **2008**, *38*, 143-172.